Spin estimations from lensing of hot spot around SMBHs

From Empiric to Deep Learning

Aristomenis Yfantis

+R. Al-Belmpeisi, D. Palumbo, M. Moscibrodzka

INSTITUTO DE ASTROFÍSICA DE ANDALUCÍA

EHT

Warsaw BH workshop
09/2026

Why

- ➢ BH creation
- ➢ Evolution
- ➢ Ergosphere
- ➢ Jets
- ➢ Its cool

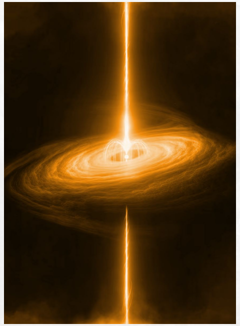

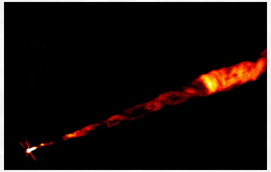

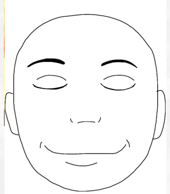

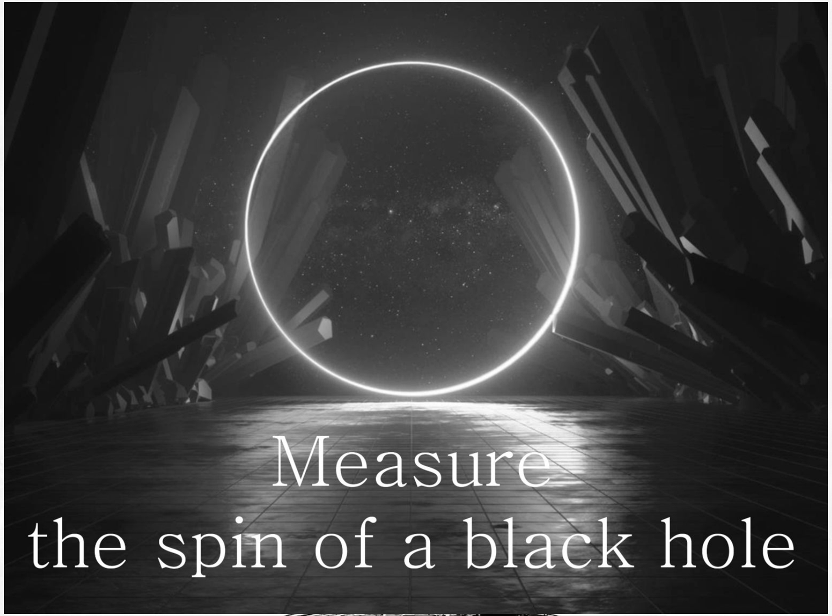

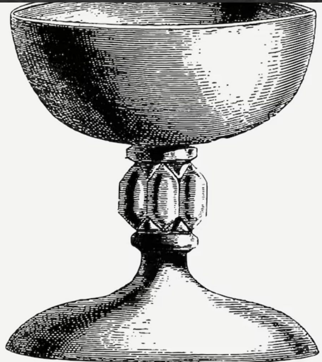

Sgr A* polarized image

- **Spin information hidden somewhere in there**

- **But deeply mixed in the physics of accretion (dirty astrophysics)**

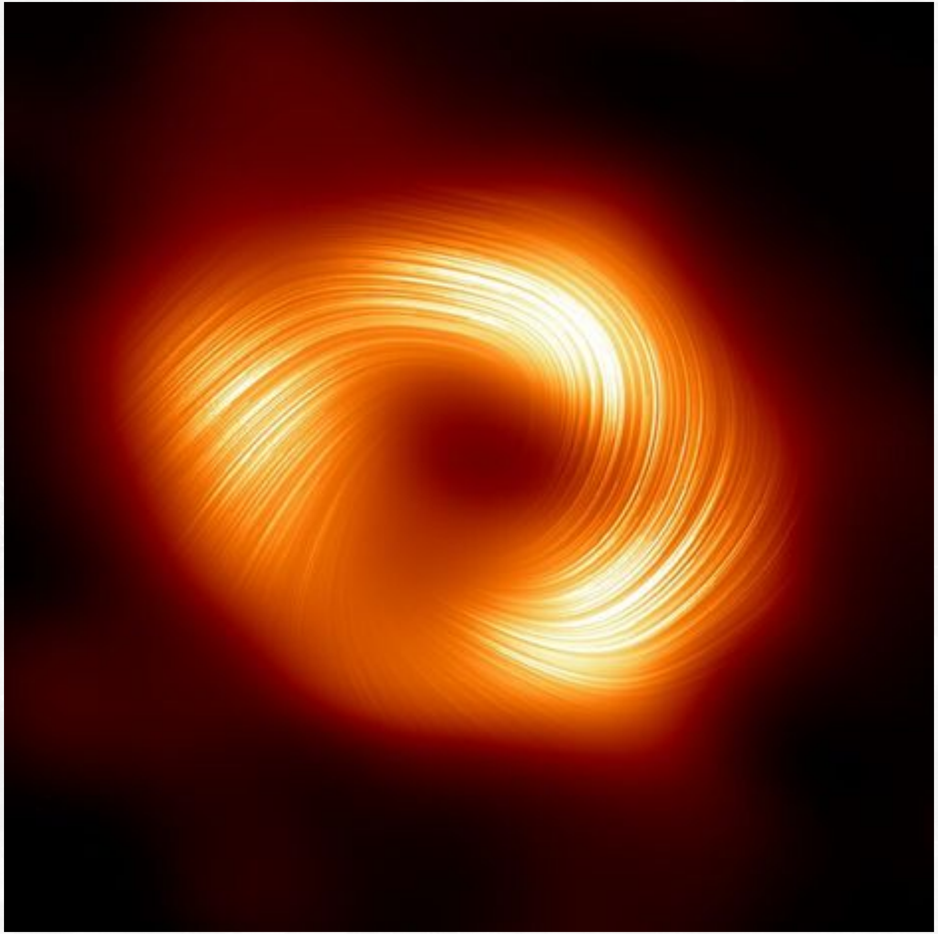

EHTC 2022

Secondary image: the photon ring

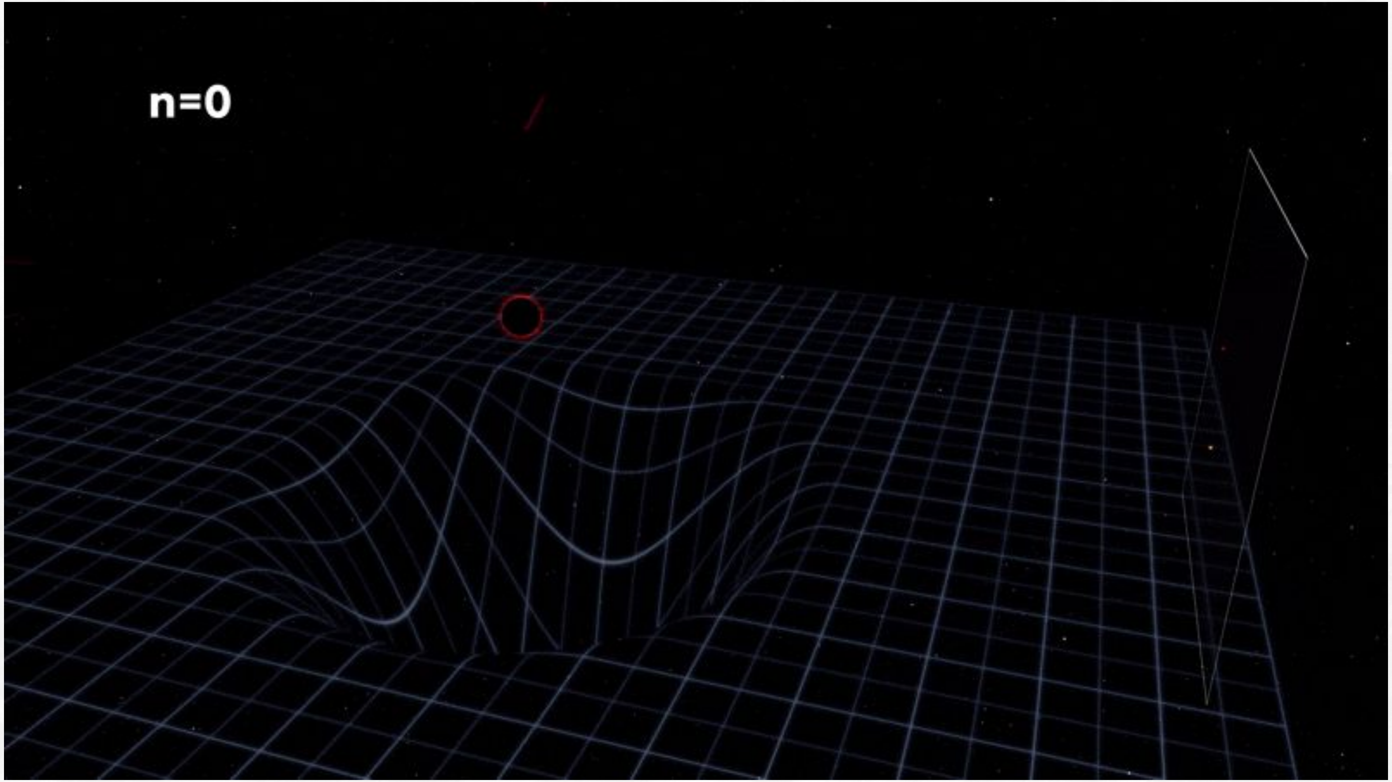

Credit: Center for Astrophysics | Harvard & Smithsonian

Secondary image: the photon ring

- **But still impossible to disentangle with current resolution**

Credit: Center for Astrophysics | Harvard & Smithsonian

Secondary image: the photon ring

- **But still impossible to disentangle with current resolution**

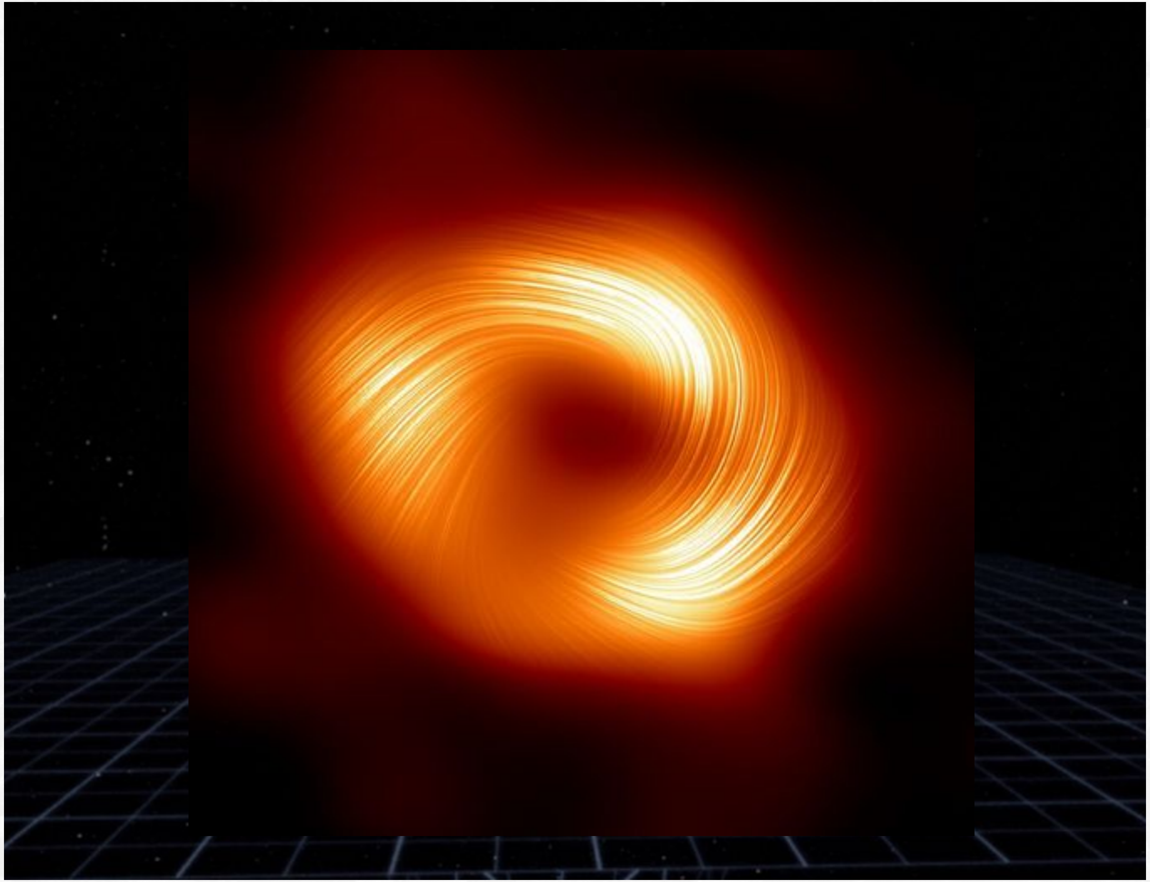

Credit: Center for Astrophysics | Harvard & Smithsonian

Why hotspot?

Credit:
EHT Collaboration, ESO/M. Kornmesser
(Acknowledgment: M. Wielgus)

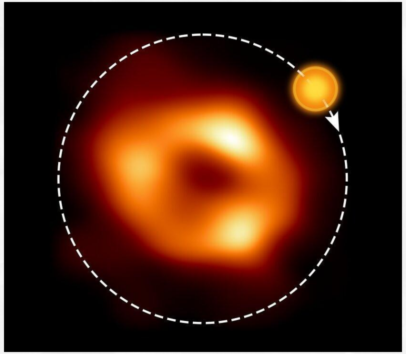

- ALMA fitting, Gravity fitting, Flares, Astrometry, Polarimetry, (VLBI?)
- Radio, NIR, Xray..

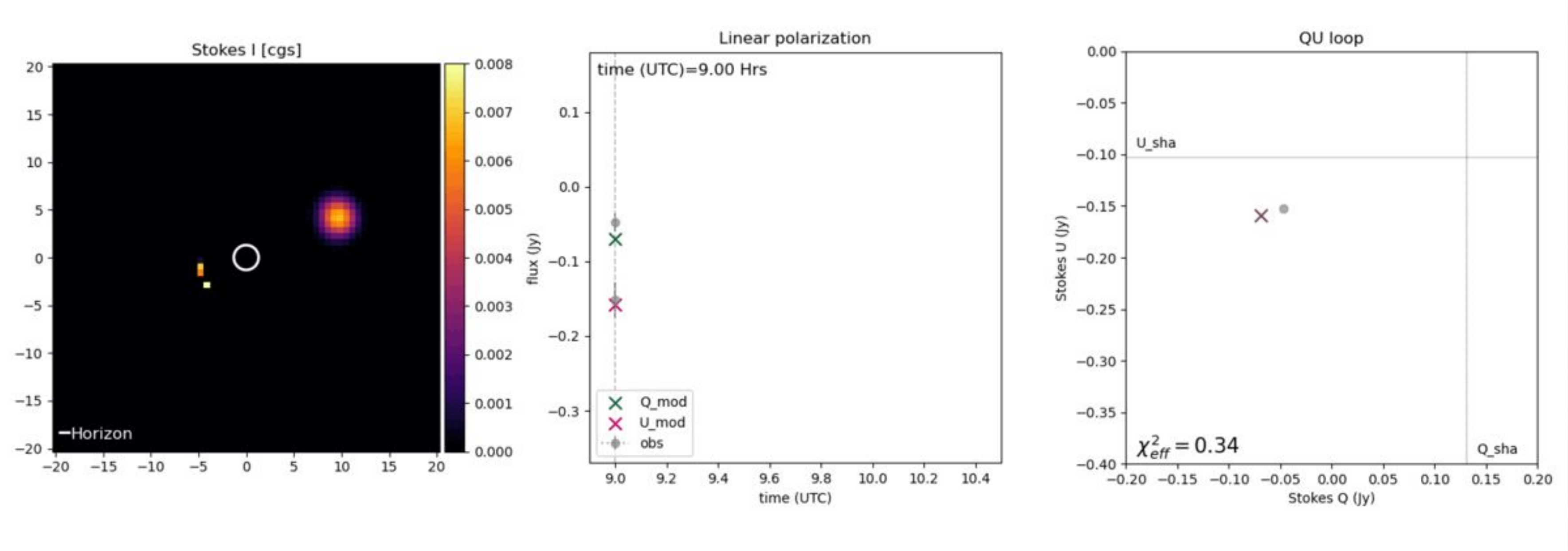

Yfantis+ 24a,b

Spin estimation from hot-spot observations

Yfantis+26

TWO SPOTS !!

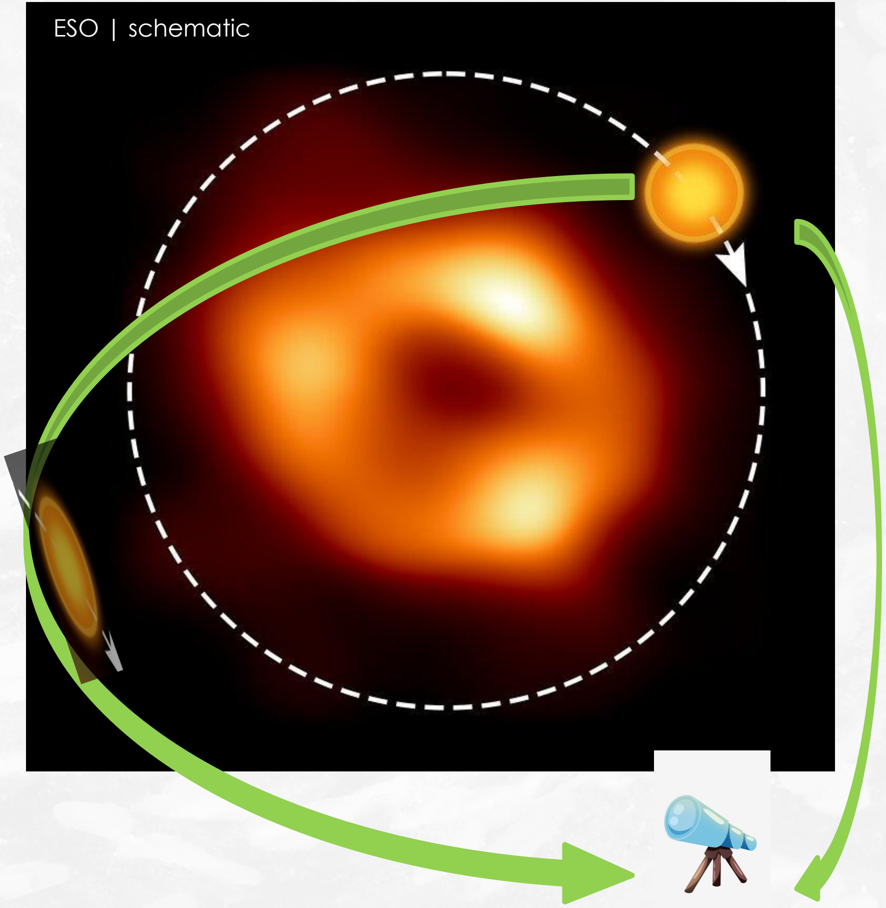

Some solutions about it..

source and observer. By integrating along the trajectory, the geodesic equation (4) may be recast in integral form,[4]

$$I_r = G_\theta, \tag{7a}$$

$$\Delta\phi := \phi_o - \phi_s = I_\phi + \lambda G_\phi, \tag{7b}$$

$$\Delta t := t_o - t_s = I_t + a^2 G_t, \tag{7c}$$

where we define

$$I_r = \fint_{r_s}^{r_o} \frac{\mathrm{d}r}{\pm_r\sqrt{\mathcal{R}(r)}}, \tag{8a}$$

$$G_\theta = \fint_{\theta_s}^{\theta_o} \frac{\mathrm{d}\theta}{\pm_\theta\sqrt{\Theta(\theta)}}, \tag{8b}$$

$$I_\phi = \fint_{r_s}^{r_o} \frac{a(2Mr - a\lambda)}{\pm_r\Delta(r)\sqrt{\mathcal{R}(r)}}\,\mathrm{d}r, \tag{8c}$$

$$G_\phi = \fint_{\theta_s}^{\theta_o} \frac{\csc^2\theta}{\pm_\theta\sqrt{\Theta(\theta)}}\,\mathrm{d}\theta, \tag{8d}$$

$$I_t = \fint_{r_s}^{r_o} \frac{r^2\Delta(r) + 2Mr(r^2 + a^2 - a\lambda)}{\pm_r\Delta(r)\sqrt{\mathcal{R}(r)}}\,\mathrm{d}r, \tag{8e}$$

$$G_t = \fint_{\theta_s}^{\theta_o} \frac{\cos^2\theta}{\pm_\theta\sqrt{\Theta(\theta)}}\,\mathrm{d}\theta. \tag{8f}$$

Here, the notation $\fint$ indicates that these integrals are to be understood as path integrals along the photon trajectory, with the signs $\pm_r = \mathrm{sign}(p^r)$ and $\pm_\theta = \mathrm{sign}(p^\theta)$ switching at radial and angular turning points, respectively. In particular, all path integrals increase monotonically along the trajectory.

A. Angular integrals

The analysis of the angular integrals differs depending on the region of conserved quantity space. In this paper, unless otherwise specified, we will restrict to positive η,

$$\eta > 0, \tag{9}$$

Gralla+ 2020

...desics with $E = 0$ exactly. ...ch an observer at infinity.

$$u_\pm = \Delta_\theta \pm \sqrt{\Delta_\theta^2 + \frac{\eta}{a^2}}, \quad \Delta_\theta = \frac{1}{2}\left(1 - \frac{\eta + \lambda^2}{a^2}\right). \tag{11}$$

To aid in the expression of the angular path integrals G_θ, G_ϕ, and G_t, we introduce the notation

$$F_i = F\left(\arcsin\left(\frac{\cos\theta_i}{\sqrt{u_+}}\right)\middle|\frac{u_+}{u_-}\right), \tag{12}$$

$$\Pi_i = \Pi\left(u_+; \arcsin\left(\frac{\cos\theta_i}{\sqrt{u_+}}\right)\middle|\frac{u_+}{u_-}\right), \tag{13}$$

$$E'_i = E'\left(\arcsin\left(\frac{\cos\theta_i}{\sqrt{u_+}}\right)\middle|\frac{u_+}{u_-}\right), \tag{14}$$

where $i \in \{s, o\}$ can be either source or observer. Here, $F(\varphi|k)$, $E(\varphi|k)$, and $\Pi(n;\varphi|k)$ respectively denote the incomplete elliptic integrals of the first, second, and third kind,[5] while the prime denotes a derivative with respect to k, $E'(\varphi|k) := \partial_k E(\varphi|k) = [E(\varphi|k) - F(\varphi|k)]/(2k)$. These integrals vanish at the equator,

$$F_i = \Pi_i = E'_i = 0, \qquad (\theta_i = 0) \tag{15}$$

and become complete at turning points,

$$F_i = \mp K, \quad \Pi_i = \mp\Pi, \quad E'_i = \mp E, \qquad (\theta_i = \theta_\pm) \tag{16}$$

where our notation for the complete elliptic integrals is

$$K = K\left(\frac{u_+}{u_-}\right) = F\left(\frac{\pi}{2}\middle|\frac{u_+}{u_-}\right), \tag{17}$$

$$\Pi = \Pi\left(u_+\middle|\frac{u_+}{u_-}\right) = \Pi\left(u_+; \frac{\pi}{2}\middle|\frac{u_+}{u_-}\right), \tag{18}$$

$$E' = E'\left(\frac{u_+}{u_-}\right) = E'\left(\frac{\pi}{2}\middle|\frac{u_+}{u_-}\right). \tag{19}$$

The $\eta > 0$ angular path integrals may be written in terms of these quantities and the number m of angular turning points encountered along the trajectory as [11, 26]

$$G_\theta = \frac{1}{a\sqrt{-u_-}}[2mK \pm_s F_s \mp_o F_o], \tag{20}$$

$$G_\phi = \frac{1}{a\sqrt{-u_-}}[2m\Pi \pm_s \Pi_s \mp_o \Pi_o], \tag{21}$$

$$G_t = -\frac{2u_+}{a\sqrt{-u_-}}[2mE' \pm_s E'_s \mp_o E'_o]. \tag{22}$$

Finally, note that the integral for G_θ can be inverted to solve for θ_o or θ_s as a function of G_θ [11, 25, 26]. Since in this paper, we mainly fix the observer point (a telescope at infinity), we present θ_s in terms of θ_o and G_θ. This may be inferred from expressions for $\theta_o(G_\theta, \theta_s)$ by interchanging s and o, before sending $G_\theta \to -G_\theta$ to compensate.[6] From Eq. (71) of Ref. [11] (noting that τ therein denotes G_θ, while ν_θ therein denotes $\pm_s$), we find

$$\frac{\cos\theta_s}{\sqrt{u_+}} = \mathrm{sn}\left(F_o \pm_o \mathrm{sign}(\eta)a\sqrt{-u_-}G_\theta\middle|\frac{u_+}{u_-}\right), \tag{25}$$

where $\mathrm{sn}(\varphi|k)$ denotes the Jacobi elliptic sine function. This formula holds regardless of the sign of η [11, 26].

B. Radial integrals

In this paper, we will consider a distant observer at

$$r_o \to \infty. \tag{26}$$

Geodesics that reach this far observer have at most one radial turning point outside the horizon. Given a choice of conserved quantities (λ, η), a simple way to test whether the ray has a turning point is to compute $r_4(\lambda, \eta)$ via Eq. (A8d) below. If r_4 is real and outside the horizon, then the ray has a turning point at radius r_4; otherwise, the ray never encounters a turning point.

For the rays with no turning point, the radial integrals I_r, I_ϕ, and I_t are single-valued functions of r_s, while for the rays with a turning point, these radial integrals must be double-valued in order to track whether or not the turning point has been reached. We will denote the number of turning points of a *photon* (portion of a ray) by $w \in \{0, 1\}$. The radial integral I_r may then be written

$$I_r = \int_{r_s}^{\infty} \frac{\mathrm{d}r}{\sqrt{\mathcal{R}(r)}} + 2w\int_{r_4}^{r_s} \frac{\mathrm{d}r}{\sqrt{\mathcal{R}(r)}}, \tag{27}$$

and likewise for I_ϕ and I_t with the appropriate integrands.[7] We may relate w to the emission direction by

$$w = \begin{cases} 0 & p_s^r > 0, \\ 1 & p_s^r < 0 \text{ (and } r_+ < r_4 < r_s). \end{cases} \tag{28}$$

[6]The future-directed geodesic from source to observer is also a past-

A ray reaching infinity origina... horizon (of the white hole) or fr... the associated radial integral I_r ...

$$I_r^{\mathrm{total}} = \begin{cases} 2\int_{r_4}^{\infty} \frac{\mathrm{d}r}{\sqrt{\mathcal{R}(r)}} \\ \int_{r_+}^{\infty} \frac{\mathrm{d}r}{\sqrt{\mathcal{R}(r)}} \end{cases}$$

where we remind the reader tha... began at infinity if $r_4(\lambda, \eta)$ is re... horizon, and otherwise began at t...

The full set of radial integrals ... duced to elliptic form in Ref. [1... work in Refs. [24, 25]. The nece... computing Eqs. (27) and (29) are...

As in Eq. (25) for $\theta_s(G_\theta)$, one ... formula for $r_s(I_r)$ [11, 25]. Eq. (... a formula for r_o, and we may inf... described above Eq. (25), i.e., b... and then sending $I_r \to -I_r$. Not... and letting $r_o \to \infty$, the emission...

$$r_s = \frac{r_4 r_{31} - r_3 r_{41}\,\mathrm{sn}^2\left(\frac{1}{2}\sqrt{r_3 \ldots}\right.}{r_{31} - r_{41}\,\mathrm{sn}^2\left(\frac{1}{2}\sqrt{r_{31} r \ldots}\right.}$$

with

$$\mathcal{F}_o = F\left(\arcsin\sqrt{\frac{r_{31}}{r_{41}}}\middle|k\right.$$

Here, we introduced the notation

$$r_{ij} = r_i - r \ldots$$

with the roots $\{r_1, r_2, r_3, r_4\}$ giv... This formula is contingent on the... in the allowed range,

$$0 < I_r < I_r^{\mathrm{to} \ldots}$$

Provided that Eq. (33) is satisf... emission radius of a photon rea... served quantities (λ, η). This fo... (some of) the radial roots are co...

C. Fractional numb...

Spin estimation from hot-spot observations

Yfantis, Palumbo, Moscibrodzka, 2026

distance (rs) velocity (Ω) BH spin (a) viewing angle (i)

1000 combinations

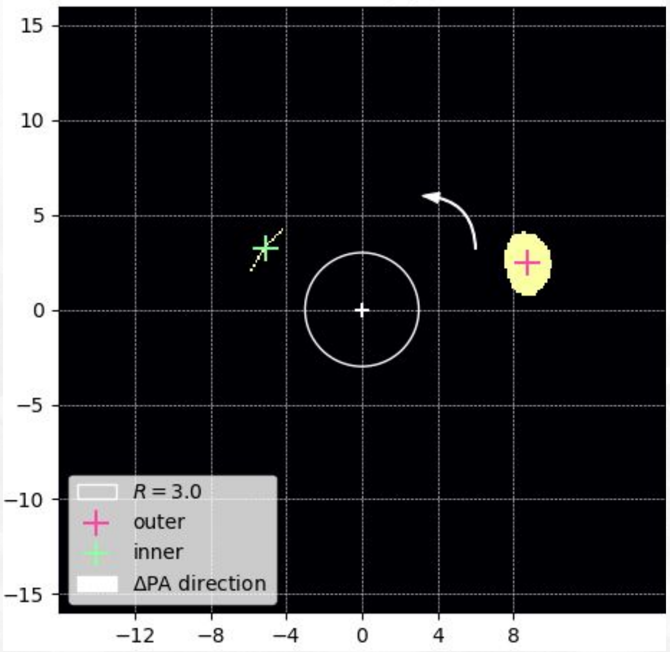

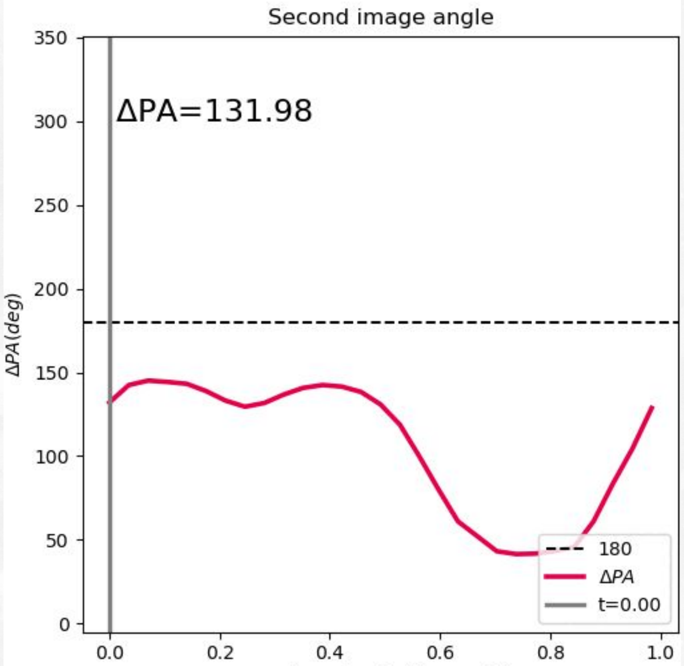

Simulations in IPOLE

Spin estimation from hot-spot observations

Yfantis, Palumbo, Moscibrodzka, 2026

distance (rs) velocity (Ω) BH spin (a) viewing angle (i)

1000 combinations

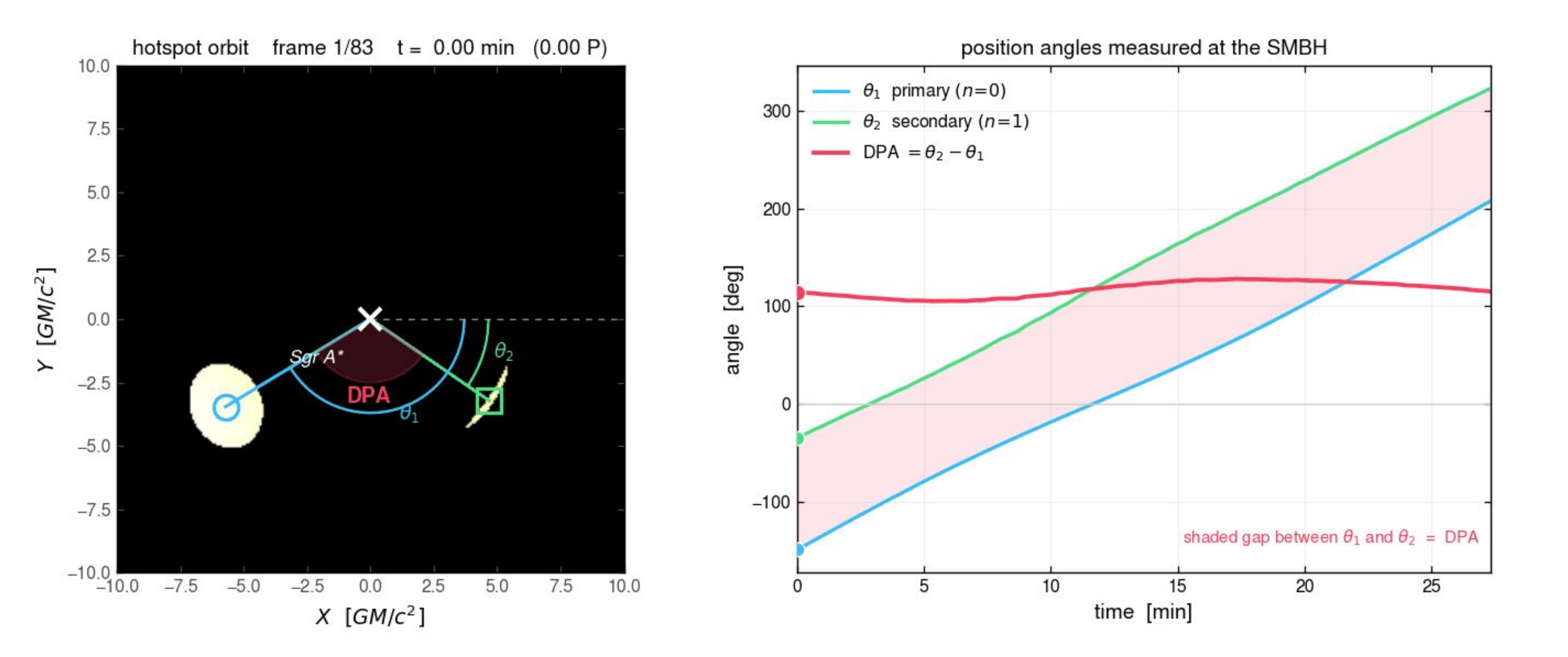

Simulations in IPOLE

□ an empirical relation*

Yfantis+ 26

BH spin

$$\Delta PA\,[deg] = 180 + a_*(40 - r_s) - \left(\frac{1408 - 233a_*}{r_s^2} + 35\right) K_{\rm coeff}$$

distance

speed

Equatorial spots
i = 0 (or avg over full period)

*Straight through pattern observations, trial-an-error and pyFit functions.

□ an empirical relation*

Yfantis+ 26

$$\Delta PA\,[deg] = 180 + a_*(40 - r_s) - \left(\frac{1408 - 233a_*}{r_s^2} + 35\right) K_{\rm coeff}$$

***Straight through pattern identification, trial-and-error and pyFit functions.**

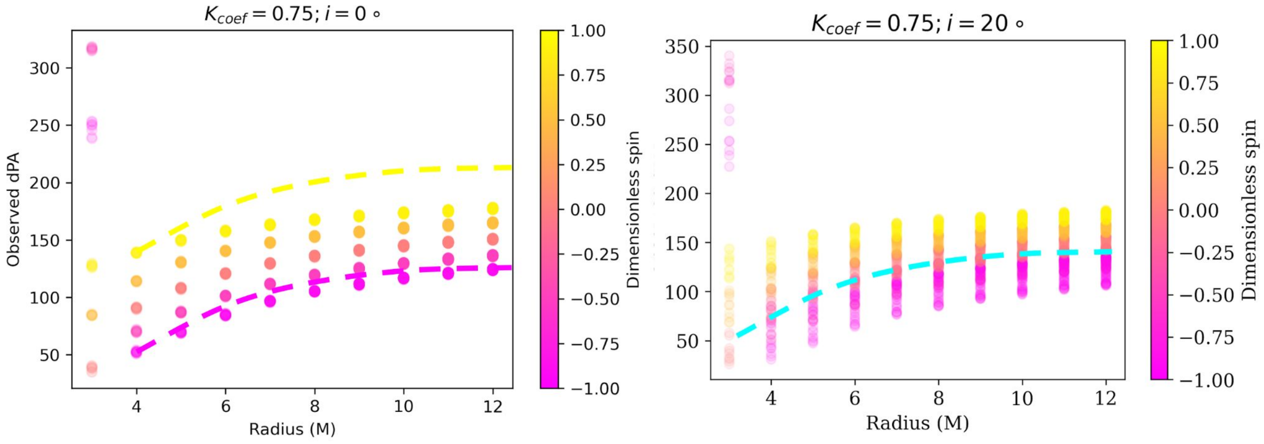

Different scaling with spin

Get rid of inclination

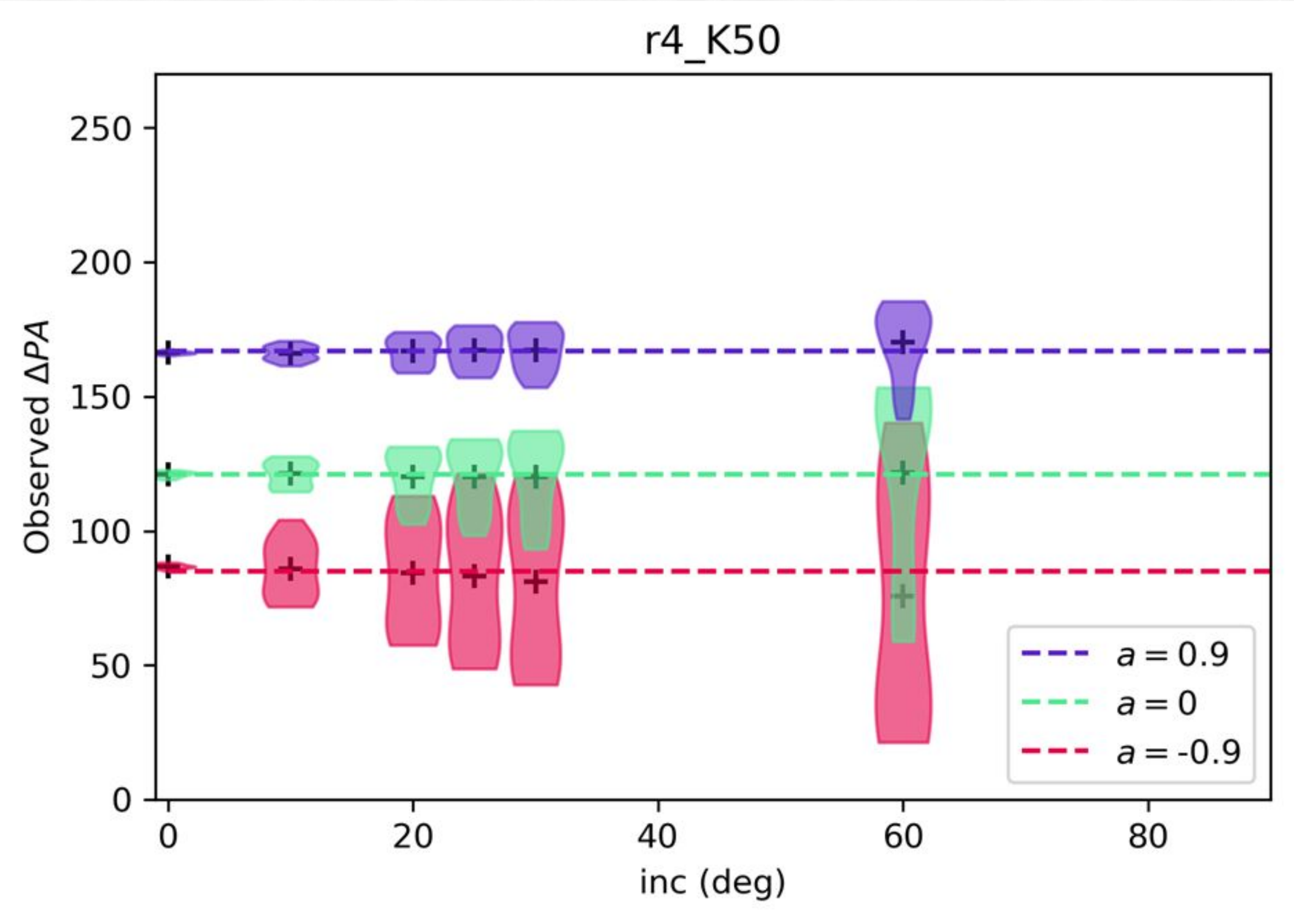

empirical relation
-comparison to analytic

$$\Delta PA\,[deg] = 180 + a_*(40 - r_s) - \left(\frac{1408 - 233a_*}{r_s^2} + 35\right) K_{\mathrm{coeff}}$$

$$\delta \mathrm{PA}_{0\to 1} = \pi + \frac{2a}{\sqrt{\tilde{b}^2 - a^2}}\left(\frac{\tilde{r}_0 + M}{\tilde{r}_0 - M}\right) \times \times K\left(\frac{\pi}{(\pi + a_* + 0.3)} \,\middle|\, \frac{a^2}{a^2 - \tilde{b}^2}\right).$$

$$\tilde{b} = \sqrt{\frac{\tilde{r}_0^3}{a_*^2}\left[\frac{4M\Delta(\tilde{r}_0)}{(\tilde{r}_0 - M)^2} - \tilde{r}_0\right] + a_*^2}.$$

$$\tilde{r}_0 = M + 2\sqrt{M^2 - \frac{a^2}{3}}\cos\left[\frac{1}{3}\arccos\left(\frac{1 - \frac{a^2}{M^2}}{\left(1 - \frac{a^2}{3M^2}\right)^{3/2}}\right)\right],$$

Performance of empiric relation

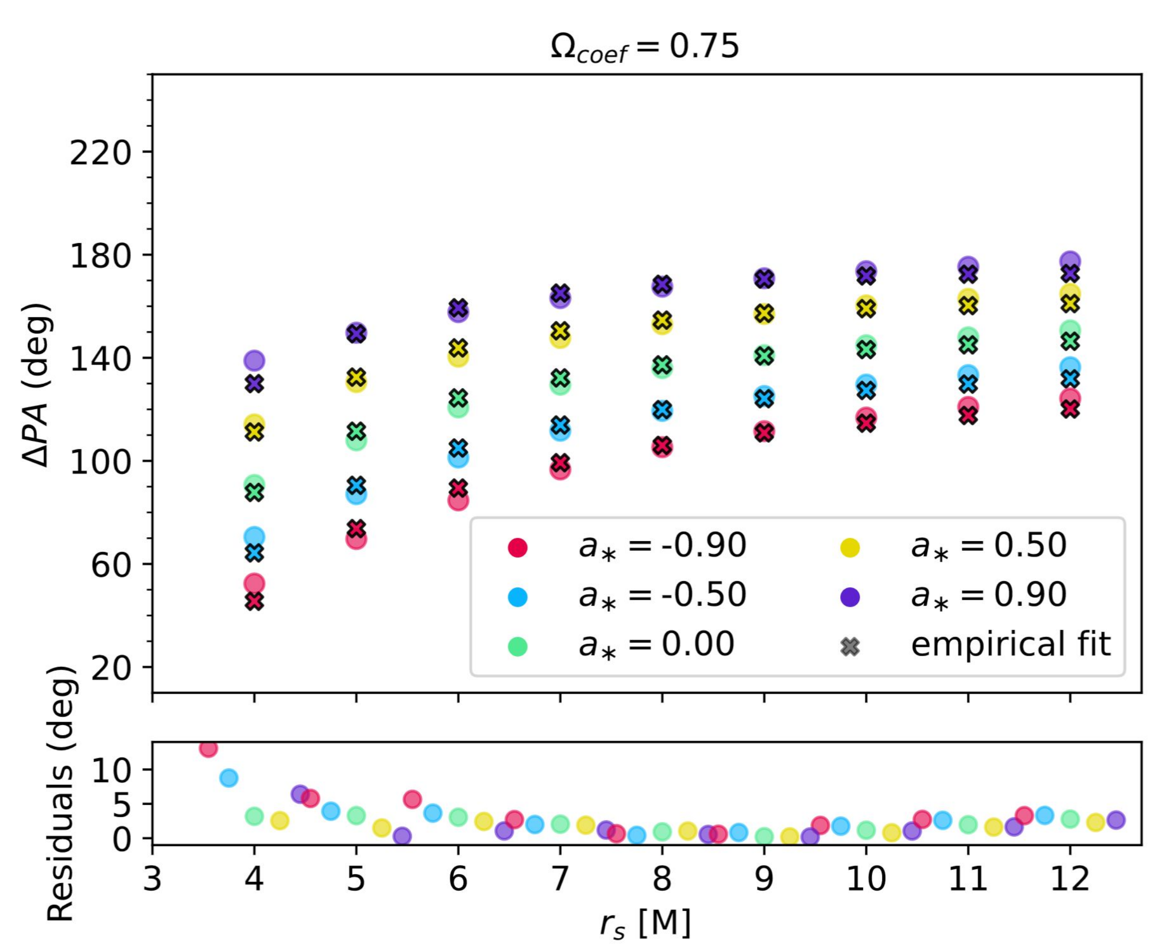

Next step

A&A, 707, A35 (2026)
https://doi.org/10.1051/0004-6361/202555277

Astronomy & Astrophysics

Lensing of hot spots in Kerr space-time

An empirical relation for black hole spin estimation

A. I. Yfantis[1,★], D. C. M. Palumbo[2,3], and M. Mościbrodzka[1]

[1] Department of Astrophysics/IMAPP, Radboud University, P.O. Box 9010, 6500 GL Nijmegen, The Netherlands
[2] Center for Astrophysics | Harvard & Smithsonian, 60 Garden Street, Cambridge, MA 02138, USA
[3] Black Hole Initiative at Harvard University, 20 Garden Street, Cambridge, MA 02138, USA

Received 23 April 2025 / Accepted 29 December 2025

Astronomy & Astrophysics manuscript no. output
May 21, 2026

In review

A deep learning algorithm for black hole spin estimation using hot-spot secondary images

A. I. Yfantis[1]* and R. Al-Belmpeisi[2]*

[1] Instituto de Astrofísica de Andalucía-CSIC, Glorieta de la Astronomía s/n, E-18008 Granada, Spain
e-mail: ayfantis@iaa.csic.es
[2] Department of Applied Mathematics and Computer Science, Technical University of Denmark, Denmark
e-mail: RAMIMAIL@eikel.dk
*Authors have contributed equally in this work.

A deep learning algorithm for black hole spin estimation using hot-spot secondary images

A. I. Yfantis[1]* and R. Al-Belmpeisi[2]*

Approximation by Superpositions of a Sigmoidal Function*

G. Cybenko†

Abstract. In this paper we demonstrate that finite linear combinations of compositions of a fixed, univariate function and a set of affine functionals can uniformly approximate any continuous function of n real variables with support in the unit hypercube; only mild conditions are imposed on the univariate function. Our results settle an open question about representability in the class of single hidden layer neural networks. In particular, we show that arbitrary decision regions can be arbitrarily well approximated by continuous feedforward neural networks with only a single internal, hidden layer and any continuous sigmoidal nonlinearity. The paper discusses approximation properties of other possible types of nonlinearities that might be implemented by artificial neural networks.

Key words. Neural networks, Approximation, Completeness.

- Deep Learning **can approximate any arbitrary function** [G. Cybenko, 1989]

Our proposed framework

STIHOS: **S**pace**T**ime **I**nference via **H**ot**S**pot **O**bservation**S**

*From the Greek στιχος = lyric

Deep Learning inference

Inputs / Observables	Inferred / Unknowns
r_{HS}	α
$\Delta PA(t)$	i
P	θ_z

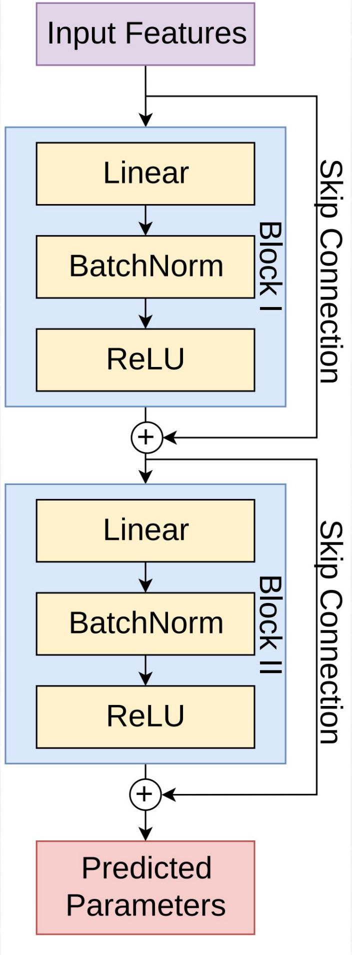

Explored Parameter Space

N = 100,000
(from 500 billion combos)

Parameter	Range	Cadence
a_*	$(-1, 1)$	0.01
r_{hs}	$[4, 12]$	0.1
Ω_{coef}	$[0.2, 1.5]$	0.1
i	$[0, 60]$	0.1
θ_z	$[-45, 45]$	1

Exp	Equatorial	Full orbit	Inputs	Predictions
I	✓	×	r, T, $\overline{\Delta PA}$	a_*
II	✓	✓	r, T, $\Delta PA(t)$	a_*, i
III	✓	×	r, T, $\Delta PA(t)$	a_*, i
IV	×	✓	r, T, $\Delta PA(t)$	a_*, i, θ_z
V	×	×	r, T, $\Delta PA(t)$	a_*, i, θ_z

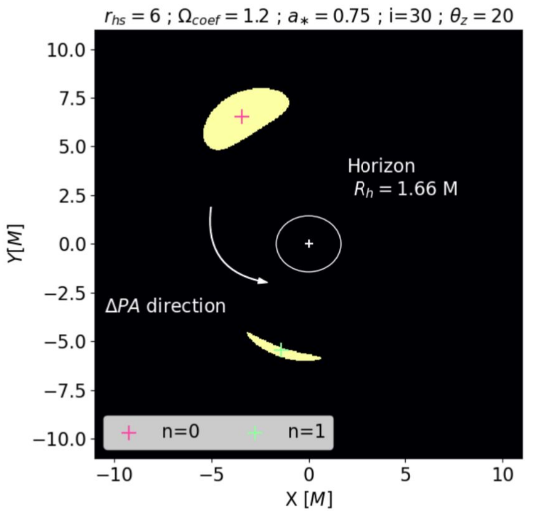

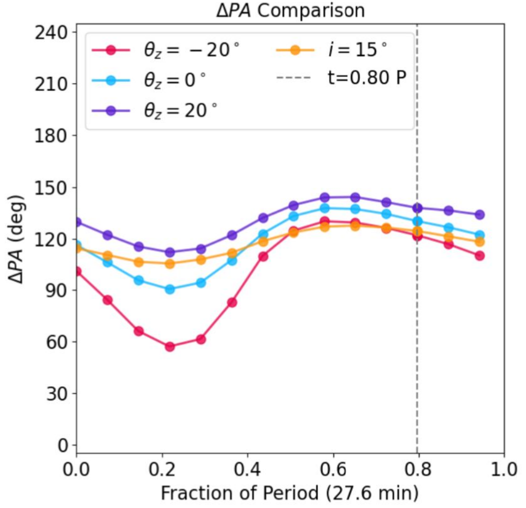

Results

Exp	Equatorial	Full orbit	Inputs	Predictions
I	✓	×	r, T, $\overline{\Delta\mathrm{PA}}$	a_*

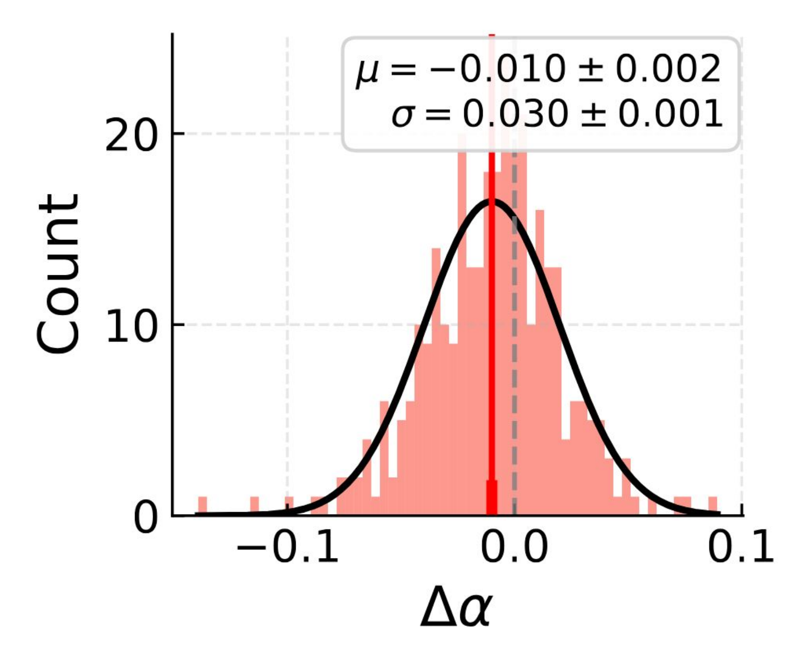

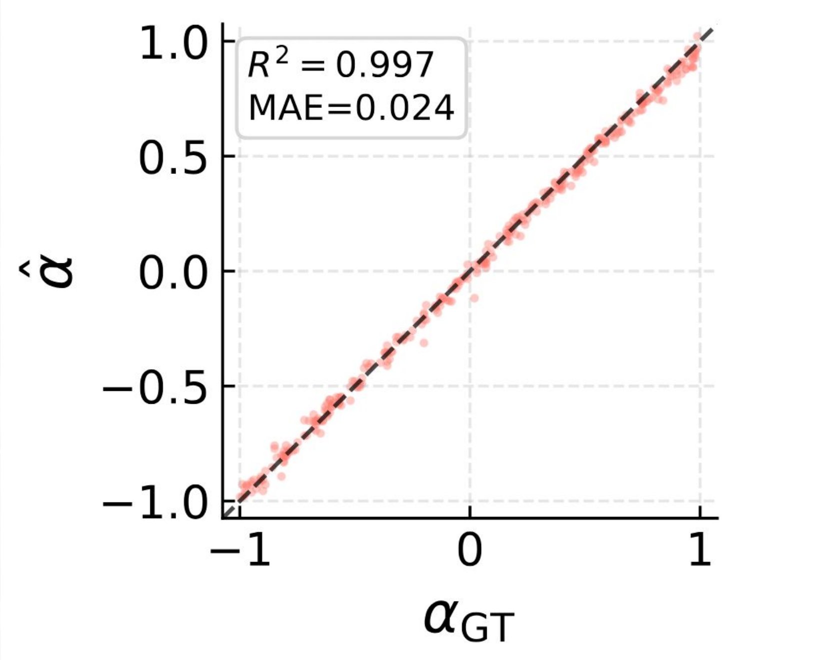

Results

Exp	Equatorial	Full orbit	Inputs	Predictions
II	✓	✓	r, T, $\Delta\mathrm{PA}(t)$	a_*, i

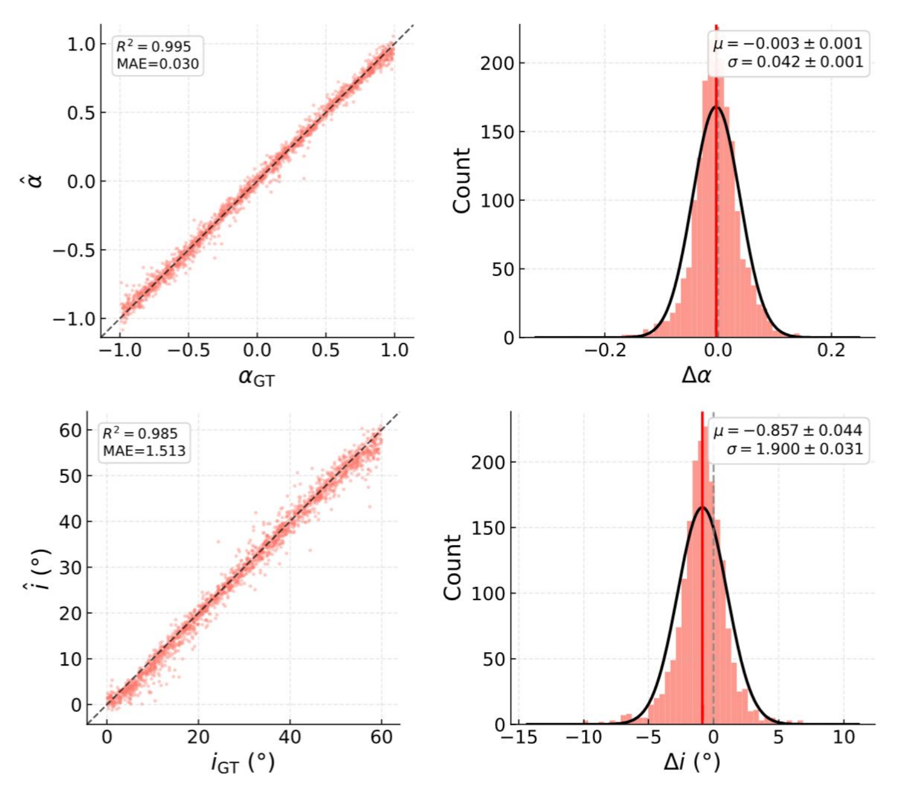

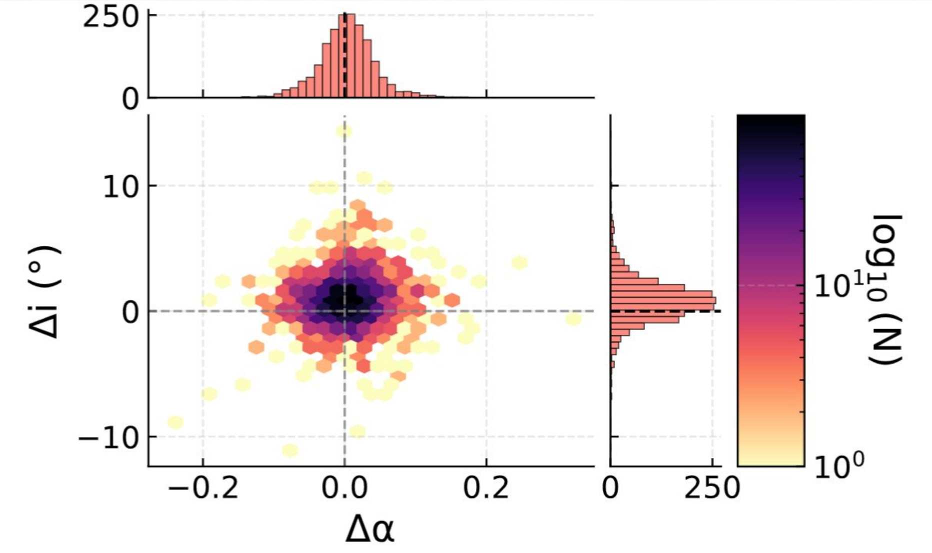

Results

Exp	Equatorial	Full orbit	Inputs	Predictions
IV	×	✓	r, T, $\Delta PA(t)$	a_*, i, θ_z

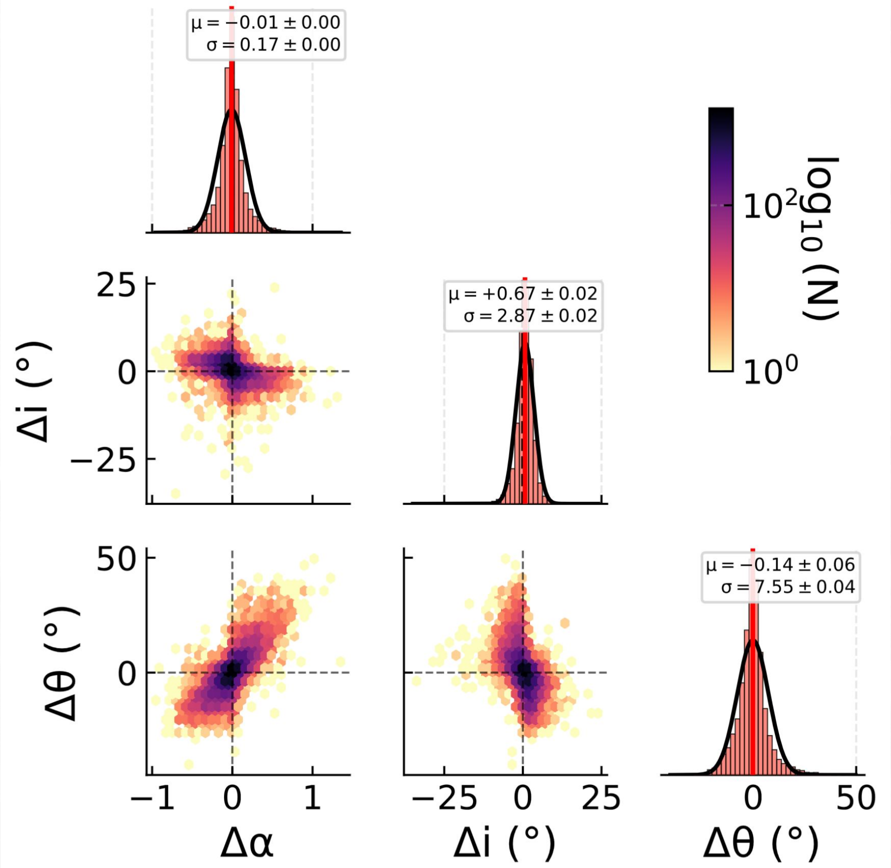

Results

Exp	Equatorial	Full orbit	Inputs	Predictions
III	✓	×	r, T, $\Delta\mathrm{PA}(t)$	a_*, i

Part of orbits (from 10% to 100%)

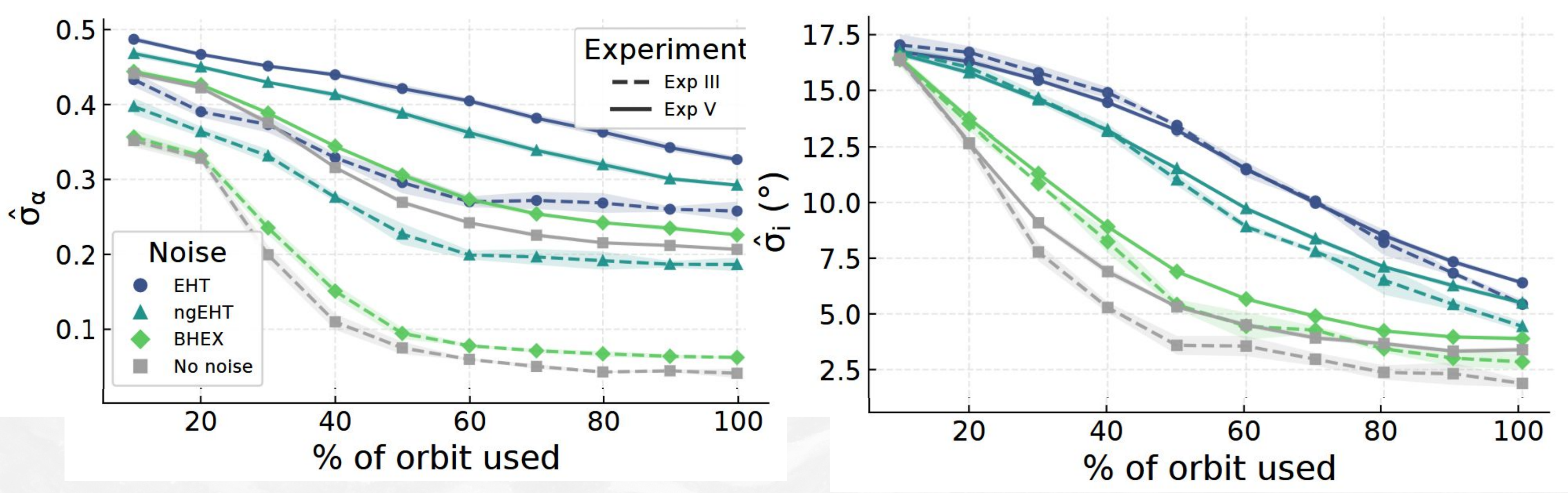

How accurate constraints can one expect from realistic observations?

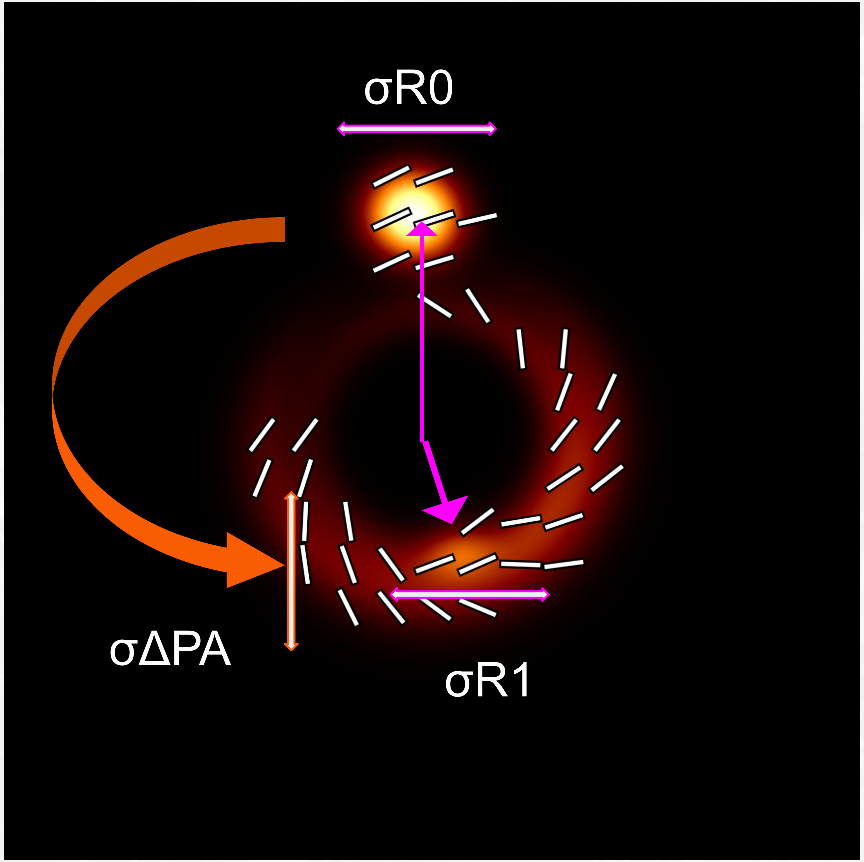

How accurate constraints can one expect from realistic observations?

Table 4. Virtual observations and assigned uncertainties.

Instrument	$\sigma_{r_{\rm hs}}$ $[M]$	$\sigma_{\Delta PA}$ $[^\circ]$	σ_P [min]
EHT	1.0	14	1
ngEHT	0.65	9	1
BHEX	0.1	2	0.5
Virtual data	r_s $[M]$	ΔPA $[^\circ]$	P [min]
1	6.0	~ 170	55
2	4.5	~ 90	30

$$\Delta PA = \arctan\left(\frac{\Delta y}{\Delta x}\right), \qquad \sigma_{\Delta PA} = \frac{2\sigma_{\Delta xy}}{L}\ \text{[rad]}.$$

$d = 51.8 \pm 2.3 \mu as$ (EHTC et al. 2022b,a)

How accurate constraints can one expect from realistic observations?

Param.	Exp.	Virtual	EHT	ngEHT	BHEX
a_*	I	1	0.31	0.21	0.05
	I	2	0.44	0.31	0.08
	II	1	0.13	0.10	0.02
	II	2	0.28	0.20	0.05
	IV	1	0.25	0.19	0.04
	IV	2	0.27	0.24	0.3
$i[^\circ]$	II	1	9.3	8.9	2.3
	II	2	7.6	4.9	1.0
	IV	1	7.9	8.2	3.8
	IV	2	5.8	4.8	1.9
$\theta_z[^\circ]$	IV	1	14	14	8.6
	IV	2	13	12	11

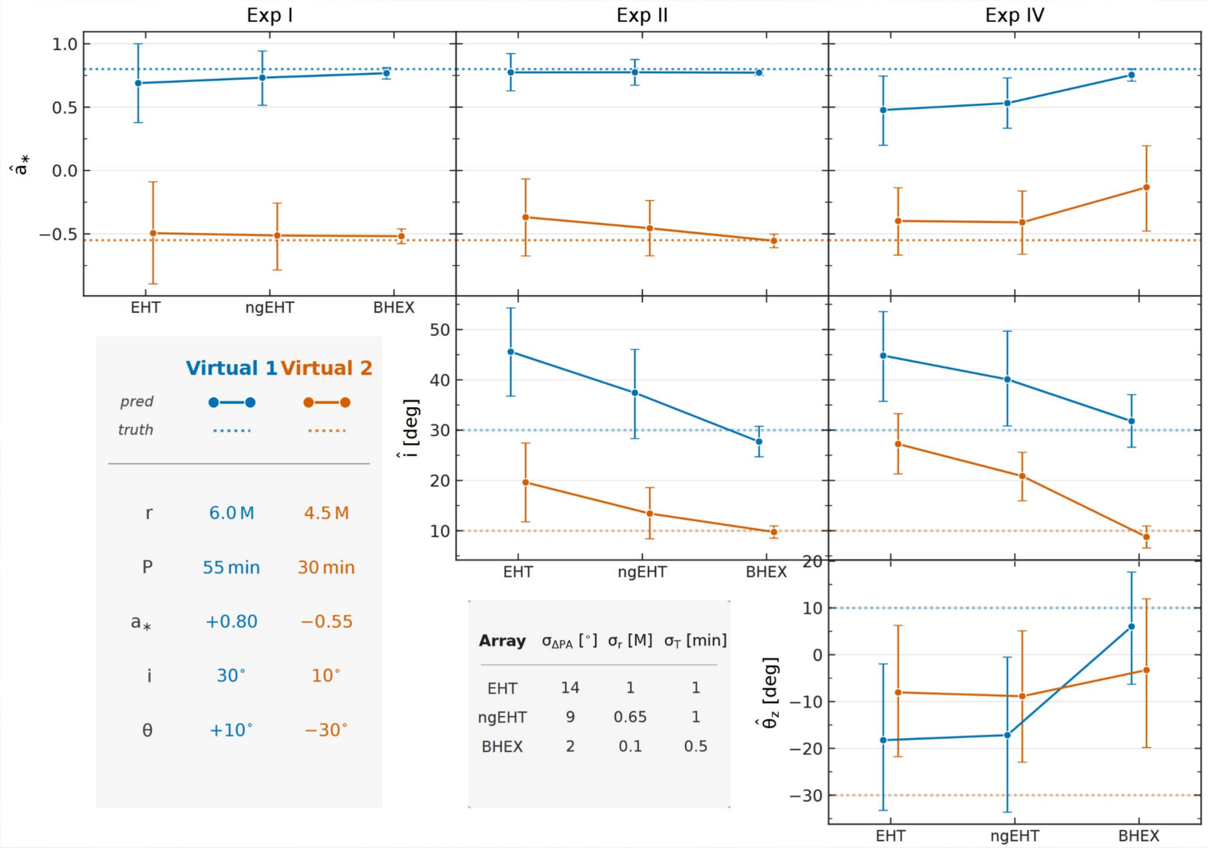

How accurate constraints can one expect from realistic observations?

Estimates can be improved from

Recurring observations

Prior info on inc, hotspot location (jet vs disk) ..

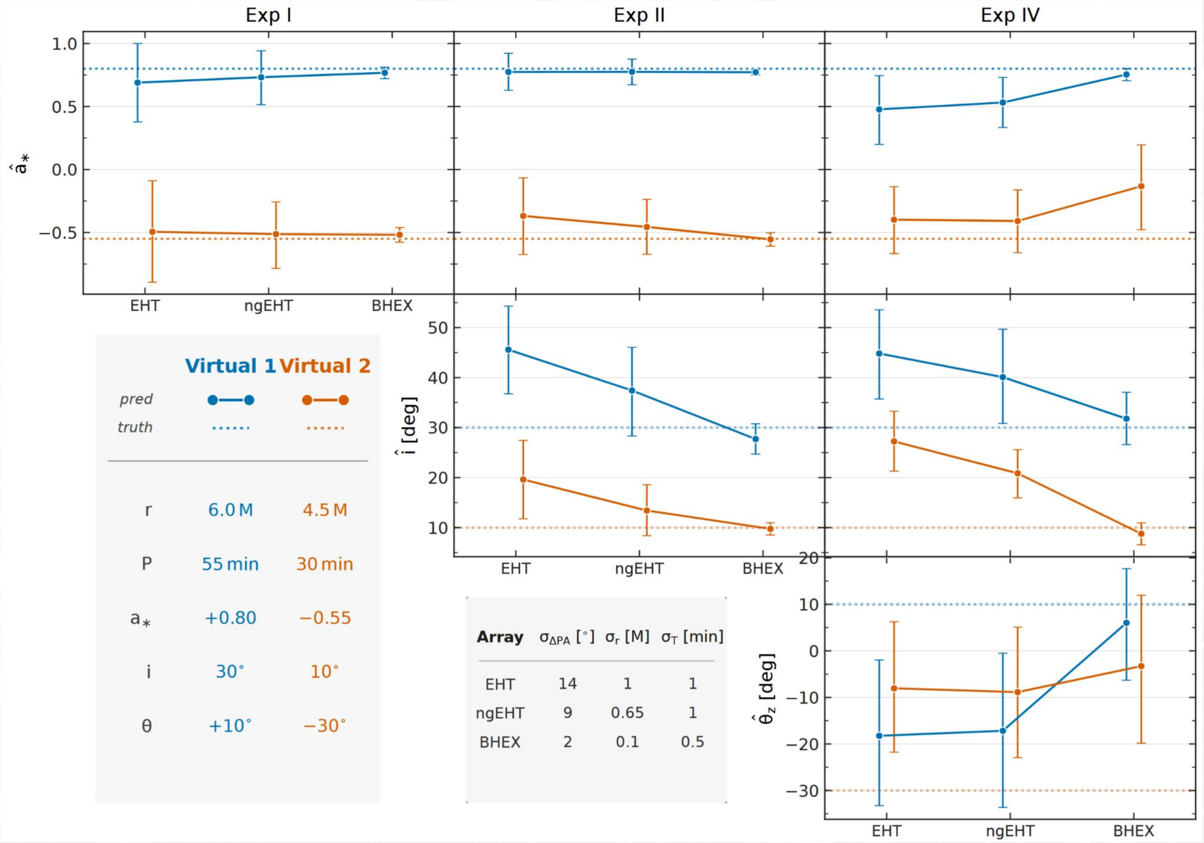

Observational feasibility
Or Looking forward

- Feature extraction: Identify hot spots
- Extract the observables (r,P,ΔPA curves)
- Study of secondary image (time delay, Intensity ratios, movement)
- Ratio of full-orbits
- Include light-curves if possible (e.g. ALMA)

STIHOS AVAILABLE AT:
https://github.com/RamiAlBel/SMBH-HotSpot-Orbits/tree/main/data

In the Future..

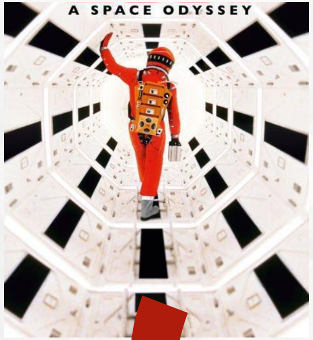

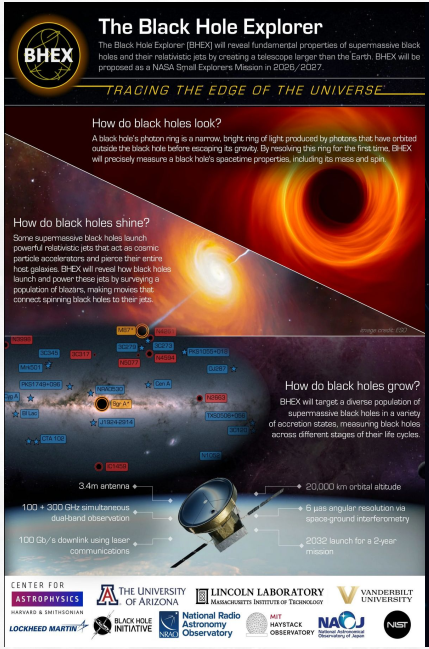

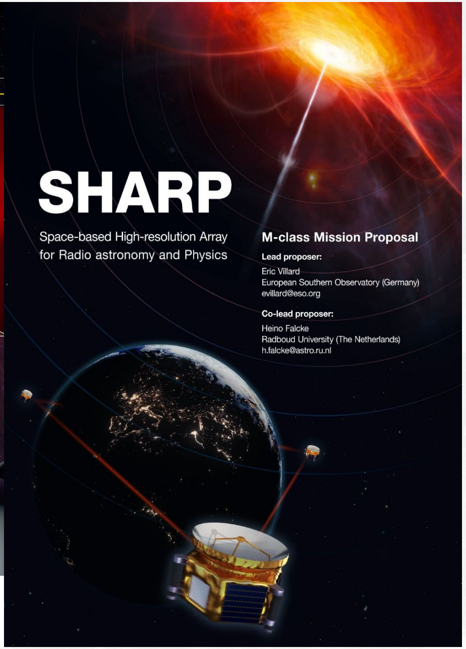

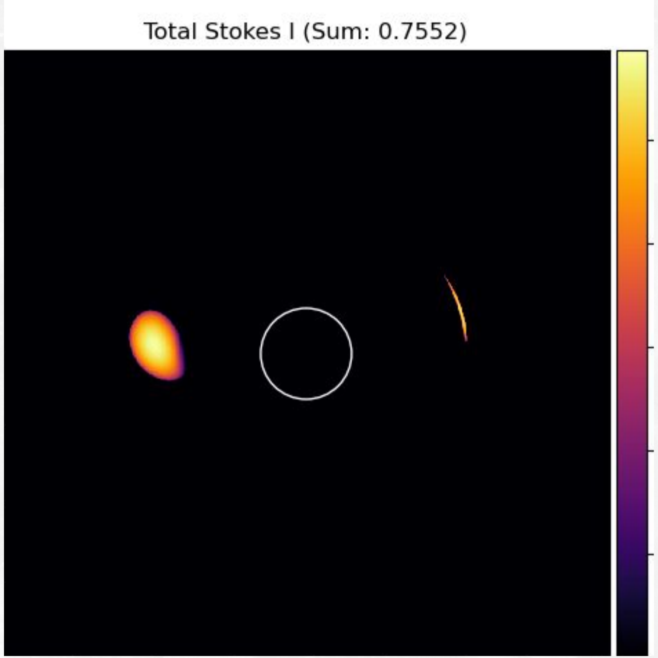

Thank you!

Spin estimations from lensing of hot spot around SMBHs

From Empiric to Deep Learning

Aristomenis Yfantis
+R. Al-Belmpeisi, D. Palumbo, M. Moscibrodzka

INSTITUTO DE ASTROFÍSICA DE ANDALUCÍA

EHT

Warsaw BH workshop
09/2026